PNAS
www.pnas.org

Supplementary Information for

Illuminating the physics of dynamic friction through laboratory earthquakes on thrust faults

Yuval Tal, Vito Rubino, Ares J. Rosakis, and Nadia Lapusta.

Ares J. Rosakis
Email: arosakis@caltech.edu

This PDF file includes:

Supplementary text
Figures S1 to S8
Tables S1
SI References

www.pnas.org/cgi/doi/10.1073/pnas.2004590117

Supplementary Information Text

S1. Laboratory setup

The laboratory setup provides full field measurements of displacements, velocities, strains, and stresses associated with dynamic shear ruptures on preexisting inclined frictional interfaces (Fig. S1). Two Homalite-100 quadrilateral plates with a frictional interface inclined at a dip angle β are loaded under uniaxial compression P (Fig. S1), resulting in initial shear and normal stresses on the interface of $\tau_0 = P\sin(\beta)\cos(\beta)$ and $\sigma_0 = P\sin^2(\beta)$, respectively. The values of β and σ_0 for the six experiments presented in the paper are shown in table S1. The rupture is nucleated by a local pressure release provided by a rapid expansion of a NiCr wire filament due to an electrical discharge of a high-voltage capacitor (Cordin 640). A key aspect of the setup is that the low shear modulus of Homalite enables to produce well-developed dynamic ruptures in samples of tens of centimeters. Once the rupture initiates, a target area coated with a random black-speckle pattern is monitored near the free-surface using an ultrahigh-speed camera system (Shimadzu HPV-X), capable of recording up to 10 million frames per second, and a high-speed white light source system with two light heads (Cordin 605) (Fig. S1). In the experiments reported here, the camera records a sequence of 128 images of the patterns distorted by the propagating rupture with a resolution of 400 x 250 pixels^2, at temporal sampling of 1 million frames/second and exposure time of 200 ns.

S2. Full-fields analysis

We employ the methodology in (1, 2) to obtain full-field maps of displacements, velocities, and stresses from the sequence of images acquired with the ultrahigh-speed camera. We analyze the images with the local digital image correlation (DIC) software Vic-2D (Correlation Solutions Inc.) to produce evolving displacement maps, computed with respect to a selected reference configuration. The 2D-DIC algorithms provide the two in-plane displacement components at each subset center. In order to capture the discontinuous displacement field across the interface, the correlation is performed separately for the domains above and below the interface. While standard local DIC approaches are able to produce the displacement map up to half a subset away from the interface, the "Fill boundary" algorithm of Vic-2D uses affine transformation functions to extrapolate the displacements from the center of the subset up to the interface. We filter the high-frequency noise from the displacement fields using a non-local-means (NL-means) filter (3–5) and have developed a post processing algorithm (6) that locally adjust the displacements computed by DIC near the interface to ensure continuity of tractions across the interface.

We employ a frame system x_1-x_2 parallel to the interface and calculate the strains from the filtered displacement fields using a finite difference approximation, with central difference scheme for pixels away from the boundaries and second-order backward and forward difference schemes at the pixels immediately above and below the interface, respectively (1, 2). The stress changes with respect to the reference configuration (before

rupture) are computed from the strain fields using the standard plane-stress linear elastic constitutive equations. Because Homalite-100 is a strain-rate sensitive material at the strain rate levels developed during the dynamic ruptures, we use the dynamic values of the elastic constants to compute the stress changes (1, 2). The actual stresses are obtained from the stress changes by adding the initial stresses. The full-field analysis enables to observe displacements, velocities, and stresses close to the interface and study how the normal (σ) and shear (τ) tractions, slip (U), and slip rate (V) evolve at any point along the interface. A more detailed description of the laboratory setup and full-fields analysis is given in (1, 2).

S3. Determining combinations of the parameters a_v, b_v, a_f, and b_f that agree with the experimental data in ref. (1)

In model 3 of the frictional response, we test a formulation of rate-and-state friction with enhanced weakening and Prakash-Clifton law, featuring weakening parameters V_w and f_w that decrease with normal stress in the form of a power law. We consider only combinations of the power law parameters a_v, b_v, a_f, and b_f that agree with the experimental data in (1). The experiments in (1) were performed with the same experimental setup, monitoring a region close to the center of the specimen. Because of the distance from the free surface, the normal stress was nearly constant and equal to the initial normal stress (σ_0).

We find the allowable combinations of the parameters a_v, b_v, a_f, and b_f by fitting results from (1) for the experiments under σ_0 = 10 MPa, within a certain tolerance, and then narrow the sets of parameters by fitting the results from (1) for σ_0 = 5.7 and 17.6 MPa. As a result, we obtain 23 combinations of the parameters a_v, b_v, a_f, and b_f, from which we search for the best fit for Exp. #1.

Lets us describe the procedure for finding the allowable combinations of the parameters a_v, b_v, a_f, and b_f in more details. For σ_0 = 10 MPa (σ_{10}), there are two sets of measurements, at $V_{\sigma 10,\mathrm{v}0.2}$ = 0.2 m/s and $V_{\sigma 10,\mathrm{v}3}$ = 3 m/s (Fig. S3). At steady-state, $L_{RS}/\theta \rightarrow V$, thus equations 2 and 3 give

$$f_{\sigma 10}(V) = f_{w,\sigma 10} + \frac{f_{RS}(V) - f_{w,\sigma 10}}{1 + \frac{V}{V_{w,\sigma 10}}}, \tag{S1}$$

where $f_{RS}(V)$ is the steady state values of RS friction. The curve in equation S1 should go through values of friction $f_{\sigma 10}(V_{\sigma 10,\mathrm{v}0.2})$ and $f_{\sigma 10}(V_{\sigma 10,\mathrm{v}3})$ that are within the experimental data. That can be achieved by choosing the enhanced weakening parameters $V_{w,\sigma 10}$ and $f_{w,\sigma 10}$ at σ_0 = 10 MPa such that they satisfy:

$$f_{w,\sigma 10} + \frac{f_{RS}(V_{\sigma 10,\mathrm{v}0.2}) - f_{w,\sigma 10}}{1 + \frac{V_{\sigma 10,\mathrm{v}0.2}}{V_{w,\sigma 10}}} = f_{\sigma 10}(V_{\sigma 10,\mathrm{v}0.2}) \tag{S2}$$

and

$$f_{w,\sigma 10} + \frac{f_{RS}(V_{\sigma 10,\mathrm{v}3}) - f_{w,\sigma 10}}{1 + \frac{V_{\sigma 10,\mathrm{v}3}}{V_{w,\sigma 10}}} = f_{\sigma 10}(V_{\sigma 10,\mathrm{v}3}), \tag{S3}$$

which give

$$V_{w,\sigma 10} = \left(f_{\sigma 10}\left(V_{\sigma 10,\mathrm{v0.2}}\right) - f_{\sigma 10}\left(V_{\sigma 10,\mathrm{v3}}\right)\right) \Big/ \left(\frac{f_{\sigma 10}\left(V_{\sigma 10,\mathrm{v0.2}}\right) - f_{RS}\left(V_{\sigma 10,\mathrm{v0.2}}\right)}{V_{\sigma 10,\mathrm{v0.2}}} - \frac{f_{\sigma 10}\left(V_{\sigma 10,\mathrm{v3}}\right) - f_{RS}\left(V_{\sigma 10,\mathrm{v3}}\right)}{V_{\sigma 10,\mathrm{v3}}}\right) \tag{S4}$$

and

$$f_{w,\sigma 10} = f_{\sigma 10}\left(V_{\sigma 10,\mathrm{v0.2}}\right) + \frac{V_{w,\sigma 10}}{V_{\sigma 10,\mathrm{v0.2}}}\left(f_{\sigma 10}\left(V_{\sigma 10,\mathrm{v0.2}}\right) - f_{RS}\left(V_{\sigma 10,\mathrm{v0.2}}\right)\right). \tag{S5}$$

Considering that the experimental data may include errors and that the interfaces of different experiments may slightly change, we allow some flexibility fitting to the experimental data of (1). We use a threshold value of ε_f = 0.03 above and below the experimental data and allow the values of $f_{\sigma 10}(V_{\sigma 10,\mathrm{v0.2}})$ and $f_{\sigma 10}(V_{\sigma 10,\mathrm{v3}})$ to range between $f_{\sigma 10,V0.2,\min}$ - ε_f and $f_{\sigma 10,V0.2,\max}$ +ε_f and between $f_{\sigma 10,V3,\min}$ - ε_f and $f_{\sigma 10,V3,\max}$ +ε_f, respectively (Fig. S4). Note that, at $V_{\sigma 10,\mathrm{v3}}$ = 3 m/s, the curve generated with V_w and f_w that are independent of σ (V_w = 1.1 m/s and f_w = 0.27) is lower than the experimental data by more than 0.03. The values of $V_{w,\sigma 10}$ and $f_{w,\sigma 10}$ for a trial pair of $f_{\sigma 10}(V_{\sigma 10,\mathrm{v0.2}})$ and $f_{\sigma 10}(V_{\sigma 10,\mathrm{v3}})$ give two constraints for the parameters a_v, b_v, a_f, and b_f:

$$V_{w,\sigma 10} = b_v {\sigma_{10}}^{a_v} \Rightarrow b_v = V_{w,\sigma 10}/{\sigma_{10}}^{a_v} \tag{S6}$$

and

$$f_{w,\sigma 10} = b_f {\sigma_{10}}^{a_f} \Rightarrow b_f = f_{w,\sigma 10}/{\sigma_{10}}^{a_f}. \tag{S7}$$

We use here σ_{10} instead of $\psi(\sigma)$ because each of the experiments in (1) was performed under constant value of $\sigma = \sigma_0$.

Then, we use the frictional data for σ_0 = 5.7 MPa ($\sigma_{5.7}$) and σ_0 = 17.6 MPa ($\sigma_{17.6}$) to provide additional constraints for the choices of the parameters a_v, b_v, a_f, and b_f for each trial pair of $V_{w,\sigma 10}$ and $f_{w,\sigma 10}$. To avoid repetition, we show in the following only the development of the constraint for σ_0 = 5.7 MPa in details. The values of $V_{w,\sigma 5.7}(a_v, b_v)$ and $f_{w,\sigma 5.7}(a_f, b_f)$ should generate a curve of $f_{\sigma 5.7}$(V) that goes through a trial value $f_{\sigma 5.7}(V_{\sigma 5.7})$ between $f_{\sigma 5.7,\min} - \varepsilon_f$ and $f_{\sigma 5.7,\max} + \varepsilon_f$, where $V_{\sigma 5.7}$ = 0.9 m/s is the average slip rate for the frictional data of $\sigma_{5.7}$ (Fig. S3). That gives the following condition:

$$f_{w,\sigma 5.7} + \frac{f_{RS}(V_{\sigma 5.7}) - f_{w,\sigma 5.7}}{1 + \frac{V_{\sigma 5.7}}{V_{w,\sigma 5.7}}} = f_{\sigma 5.7}(V_{\sigma 5.7}), \tag{S8}$$

where $f_{RS}(V_{\sigma 5.7})$ is the steady state values of RS friction for $V_{\sigma 5.7}$. Substituting $V_{w,\sigma 5.7} = b_v {\sigma_{5.7}}^{a_v}$ and $f_{w,\sigma 5.7} = b_f {\sigma_{5.7}}^{a_f}$ gives

$$b_f {\sigma_{5.7}}^{a_f} + \frac{f_{RS}(V_{\sigma 5.7}) - b_f {\sigma_{5.7}}^{a_f}}{1 + \frac{V_{\sigma 5.7}}{b_v {\sigma_{5.7}}^{a_v}}} = f_{\sigma 5.7}(V_{\sigma 5.7}), \tag{S9}$$

which together with the constraints in equations S6 and S7 becomes:

$$f_{w,\sigma 10}\left(\frac{\sigma_{5.7}}{\sigma_{10}}\right)^{a_f}+\frac{f_{RS}(V_{\sigma 5.7})-f_{w,\sigma 10}\left(\frac{\sigma_{5.7}}{\sigma_{10}}\right)^{a_f}}{1+\frac{V_{\sigma 5.7}}{V_{w,\sigma 10}\left(\frac{\sigma_{5.7}}{\sigma_{10}}\right)^{a_v}}}=f_{\sigma 5.7}(V_{\sigma 5.7}). \tag{S10}$$

With some algebra:

$$\left(\frac{\sigma_{5.7}}{\sigma_{10}}\right)^{a_f}=\frac{f_{\sigma 5.7}(V_{\sigma 5.7})\left(1+\frac{V_{\sigma 5.7}}{V_{w,\sigma 10}}\left(\frac{\sigma_{5.7}}{\sigma_{10}}\right)^{a_v}\right)(V_{\sigma 5.7})-f_{RS}(V_{\sigma 5.7})}{\frac{V_{\sigma 5.7}}{V_{w,\sigma 10}}\left(\frac{\sigma_{5.7}}{\sigma_{10}}\right)^{a_v}} \tag{S11}$$

and an expression for a_f is obtained:

$$a_f=\log\left[\frac{f_{\sigma 5.7}(V_{\sigma 5.7})\left(1+\frac{V_{\sigma 5.7}}{V_{w,\sigma 10}}\left(\frac{\sigma_{5.7}}{\sigma_{10}}\right)^{a_v}\right)(V_{\sigma 5.7})-f_{RS}(V_{\sigma 5.7})}{\frac{V_{\sigma 5.7}}{V_{w,\sigma 10}}\left(\frac{\sigma_{5.7}}{\sigma_{10}}\right)^{a_v}}\right]/\log\left(\frac{\sigma_{5.7}}{\sigma_{10}}\right) \tag{S12}$$

Similarly, for σ_0 = 17.6 MPa, the values of $V_{w,\sigma 17.6}(a_v, b_v)$ and $f_{w,\sigma 17.6}(a_f, b_f)$ should generate a curve of $f_{\sigma 17.6}(\mathrm{V})$ that goes through a trial value $f_{\sigma 17.6}(V_{\sigma 17.6})$ between $f_{\sigma 17.6,\min}-\varepsilon_f$ and $f_{\sigma 17.6,\max}+\varepsilon_f$. That provides another expression for a_f:

$$a_f=\log\left[\frac{f_{\sigma 17.6}(V_{\sigma 17.6})\left(1+\frac{V_{\sigma 17.6}}{V_{w,\sigma 10}}\left(\frac{\sigma_{17.6}}{\sigma_{10}}\right)^{a_v}\right)(V_{\sigma 17.6})-f_{RS}(V_{\sigma 17.6})}{\frac{V_{\sigma 17.6}}{V_{w,\sigma 10}}\left(\frac{\sigma_{17.6}}{\sigma_{10}}\right)^{a_v}}\right]/\log\left(\frac{\sigma_{17.6}}{\sigma_{10}}\right). \tag{S13}$$

For a given combination of trial values $f_{\sigma 10}(V_{\sigma 10,\mathrm{v0.2}})$, $f_{\sigma 10}(V_{\sigma 10,\mathrm{v3}})$, $f_{\sigma 5.7}(V_{\sigma 5.7})$, and $f_{\sigma 17.6}(V_{\sigma 17.6})$, we use equations S4, S5, S12 , and S13 and solve numerically for a_v and a_f, using Matlab function "*fzero*". Note that not all the combinations of trial values provide valid solutions for the parameters a_v and a_f. In cases where a solution exists and $a_v<0$ and $a_f<0$, we use equations S6 and S7 to obtain b_v and b_f. We test 5 values of $f_{\sigma 10}(V_{\sigma 10,\mathrm{v0.2}})$ between $f_{\sigma 10,V0.2,\min}$ - ε_f and $f_{\sigma 10,V0.2,\max}$ + ε_f, 4 values of $f_{\sigma 10}(V_{\sigma 10,\mathrm{v3}})$ between $f_{\sigma 10,V3,\min}$ - ε_f and $f_{\sigma 10,V3,\max}$ + ε_f, 7 values of $f_{\sigma 5.7}(V_{\sigma 5.7})$ between $f_{\sigma 5.7,\min}-\varepsilon_f$ and $f_{\sigma 5.7,\max}+\varepsilon_f$, and 4 values of $f_{\sigma 17.6}(V_{\sigma 17.6})$ between $f_{\sigma 17.6,\min}-\varepsilon_f$ and $f_{\sigma 17.6,\max}+\varepsilon_f$, all at intervals of Δf = 0.01. That gives a total of 560 combinations. However, only 23 combinations provide an allowable set of the parameters a_v, b_v, a_f, and b_f that generate three curves $f(V,\sigma_0)$, for σ_0 = 5.7, 10, and 17.6 MPa, that are all within the defined limit of 0.03 from experimental data in (1) (Figs. S5A and S5B). The parameters a_v and a_f decrease linearly with the logarithms of b_v and b_f, respectively (Fig. S5C), while there is no clear relationship between a_v and a_f (Fig. S5D).

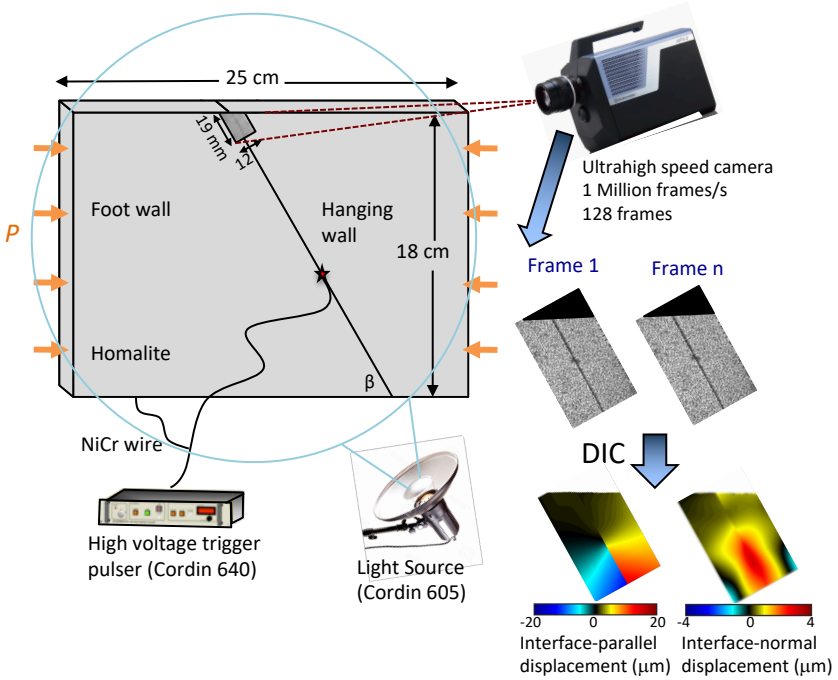

Fig. S1. Schematics of the laboratory setup. Dynamic shear ruptures evolve spontaneously along a frictional interface inclined at a dip angle β between two Homalite plates under a compressional load P. Ruptures are initiated by the small burst of a NiCr wire placed across the interface and connected to a capacitor bank. The white light produced by a flash source is reflected by the specimen's surface and captured by a low-noise high-speed camera at 1 million frames/sec. A 19 x 12 mm^2 region to be imaged is coated by a flat white paint and decorated by a characteristic speckle pattern used for image correlation.

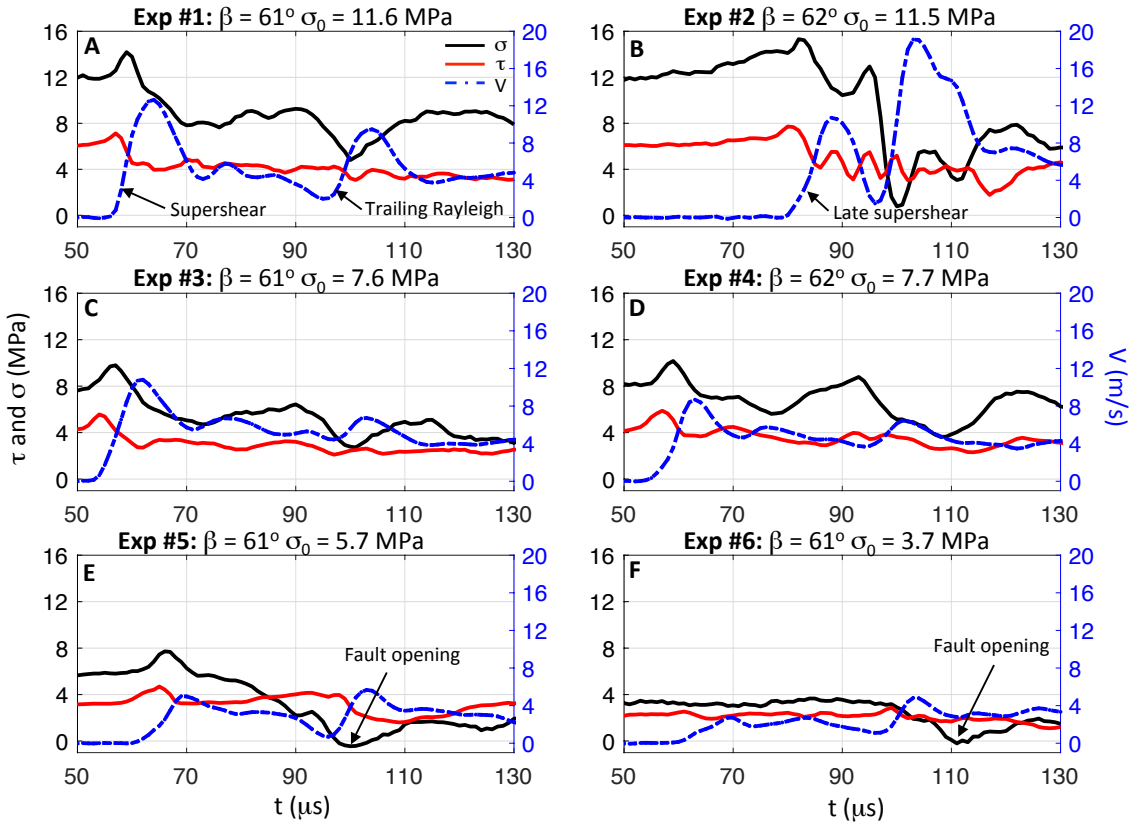

Fig. S2. Local behavior of the ruptures near the free surface in all six experiments. (**A** to **F**) The temporal evolution of τ (red), σ (black), and V (blue) at about 1.5 mm from the free surface for six experiments performed under different values of β and σ_0**.** The curves are generated using a temporal moving average, with a width of three data points, on the local data for each quantity.

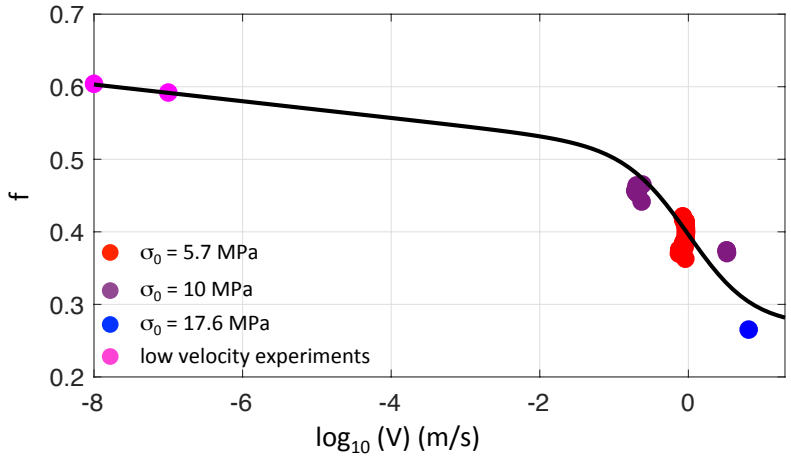

Fig. S3. The steady-state values of f vs. V in the experiments in (19) that were monitored with a small field of view and had slip rates larger than 0.1 m/s, as well as two low-velocity measurements that were obtained in a different set of experiments in (35). The data was fitted in (19) with friction model 1, that is, a combined formulation of RS friction enhanced by flash heating with the weakening parameters V_w = 1.1 m/s, and f_w = 0.27 (black curve).

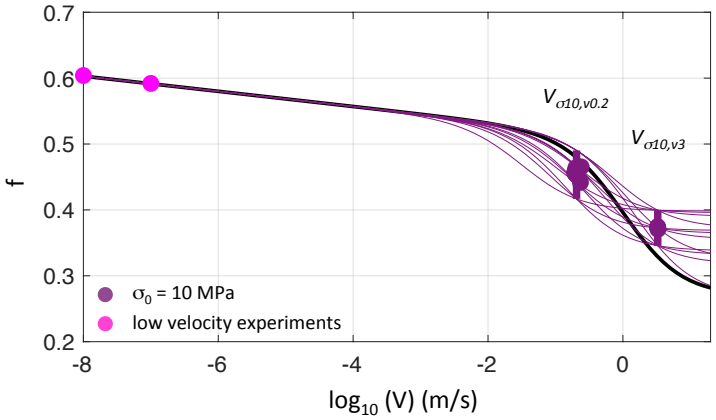

Fig. S4. Step 1 of choosing combinations of the parameters a_v, b_v, a_f, and b_f for friction model 3 that agree with the experimental data in the study of (19): fitting data for σ_0 = 10 MPa (purple curves). The curves have to go through values $f_{\sigma 10}(V_{\sigma 10,\mathrm{v}0.2})$ at $V_{\sigma 10,\mathrm{v}0.2}$ = 0.2 m/s and $f_{\sigma 10}\left(V_{\sigma 10,\mathrm{v}3}\right)$ at $V_{\sigma 10,\mathrm{v}3}$ = 3 m/s that are between threshold values of ε_f = 0.03 above and below the experimental data.

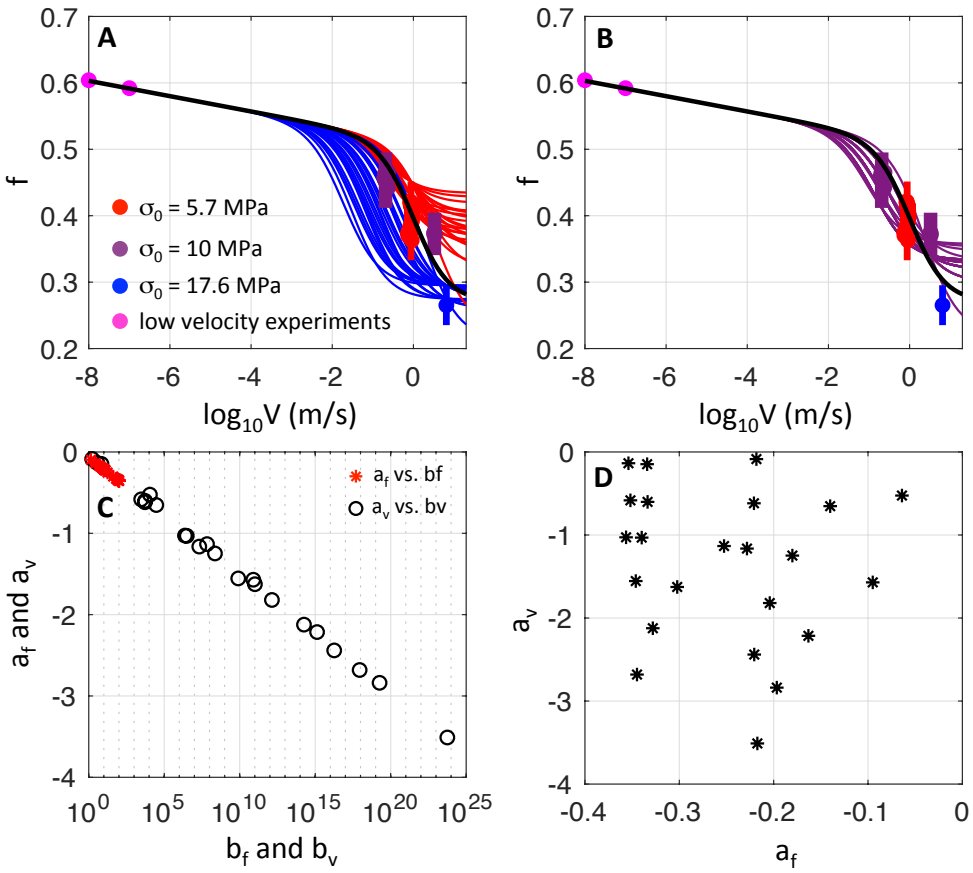

Fig. S5. Step 2 of choosing combinations of the parameters a_v, b_v, a_f, and b_f for friction model 3 that agree with the experimental data in the study of (19): fitting data for σ_0 = 5.7 and 17.6 MPa (purple curves). (A) $f(V, \sigma_0)$ curves for σ_0 = 5.7 (red) and 17.6 (blue) MPa for each of the 23 allowable combinations of the parameters a_v, b_v, a_f, and b_f. Each of the curves for a given σ_0 must go between values of ε_f above and below the experimental measurements of friction for that σ_0 (the thick vertical lines). (B) $f(V, \sigma_0)$ curves for σ_0 = 10 MPa (purple) for the 23 allowable combinations of the parameters a_v, b_v, a_f, and b_f. The black curve in (A) and (B) represents a fit with V_w = 1.1 m/s and f_w = 0.27, assuming that the weakening parameters are independent on normal stress (Model 1). (C) The parameters a_v vs. b_v (black) and a_f vs. b_f (red) for each of the allowable combinations. (D) a_v vs. a_f (black) for each of the allowable combinations.

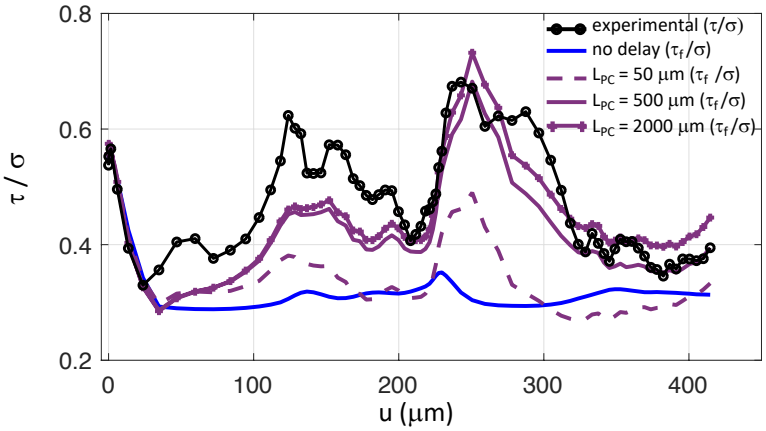

Fig. S6. Comparison of the observed response in Exp. # 1 with friction models 1 and 2. (A) Effective frictional resistance vs. slip at point on the interface located 1.5 mm from the free surface: measurements and fits with the friction models. The black circles represent the experimental measurements (smoothed by a moving average of three data points) of the ratio between the observed shear and normal tractions, τ/σ. The blue curve represents a calculated τ_f/σ ratio using enhanced-weakening RS friction without a Prakash-Clifton formulation (model 1), while the purple curves represent τ_f/σ ratios obtained with a Prakash-Clifton formulation (model 2) with different values of L_{PC}.

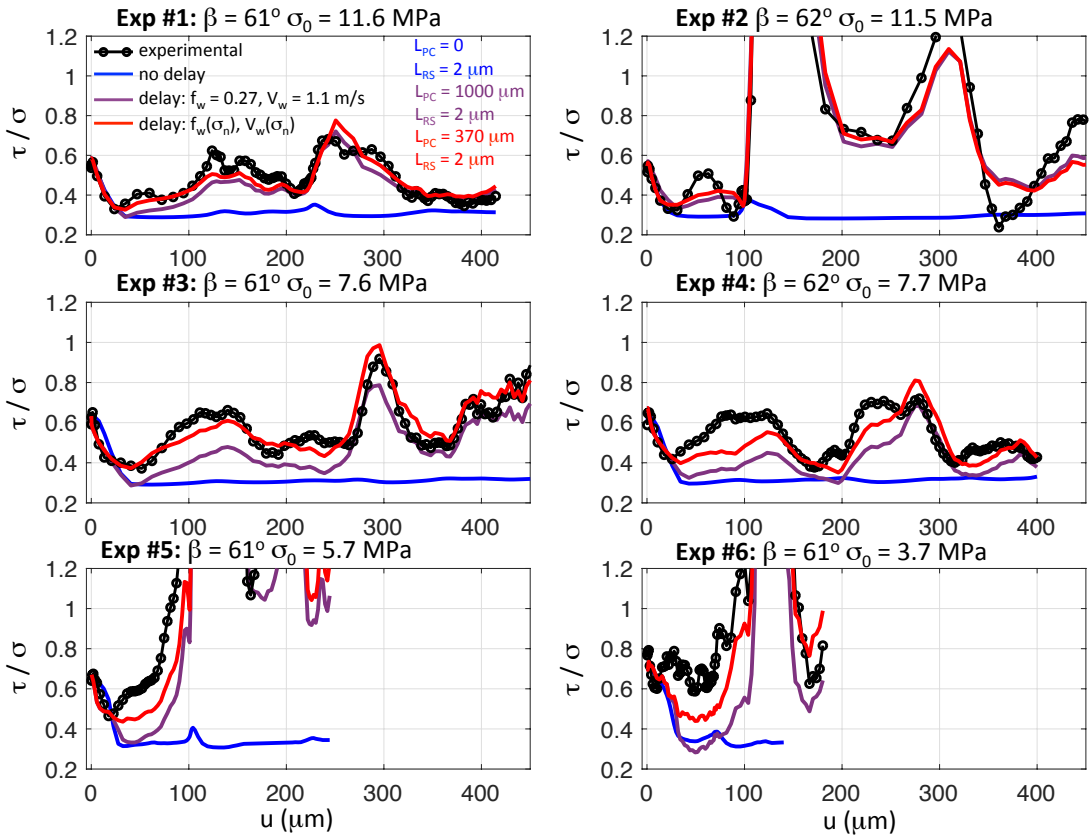

Fig. S7. Fitting Exp. #2-6 with the parameters constrained with the data in Exp. #1. Measured effective friction (black circles) and modeled effective friction estimated with model 1 (blue), model 2 (purple), and model 3 (red) vs. slip at point on the interface located 1.5 mm from the free surface. The parameters constrained with the data in Exp. #1 allow us to predict the non-trivial friction evolution in the other experiments. All experiments are best fit by friction model 3.

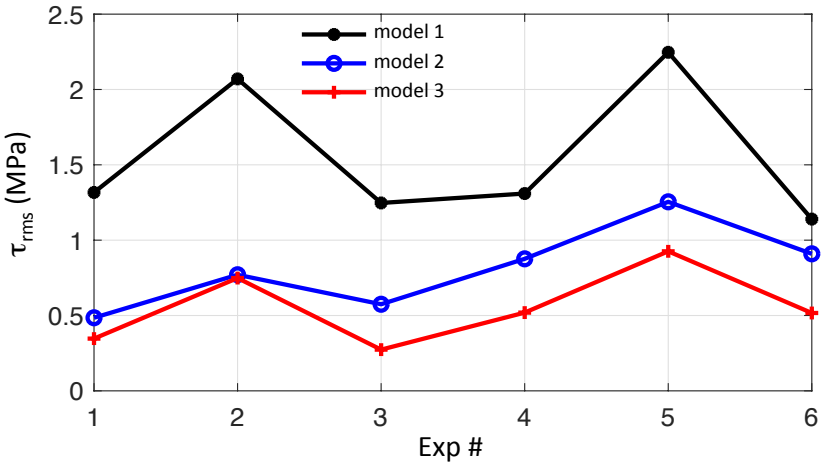

Fig. S8. The minimum RMS of the differences between the measured shear stress τ and its fits τ_f in all six experiments for friction models 1 (black), 2 (blue), and 3 (red). The values of τ_f for Exp. # 2-6 were computed using the parameters constrained with the data in Exp. #1 for each model. We use here the RMS of the shear stresses instead of the effective friction because σ decreases temporarily to zero during Exp. #5 and #6 and it is problematic to use the values of the effective friction at those stages.

Table S1. Dip angle and initial normal stress for Exp. # 1-6.

Experiment #	Dip angle β	Initial normal stress σ_0
1	61°	11.6 MPa
2	62 °	11.5 MPa
3	61 °	7.6 MPa
4	62 °	7.7 MPa
5	61 °	5.7 MPa
6	61 °	3.7 MPa

SI References

1. V. Rubino, A. J. Rosakis, N. Lapusta, Understanding dynamic friction through spontaneously evolving laboratory earthquakes. *Nat. Commun.* **8**, 1–12 (2017).
2. V. Rubino, A. J. Rosakis, N. Lapusta, Full-field ultrahigh-speed quantification of dynamic shear ruptures using digital image correlation. *Exp. Mech.* (2019).
3. V. Rubino, N. Lapusta, A. J. Rosakis, S. Leprince, J. P. Avouac, Static Laboratory Earthquake Measurements with the Digital Image Correlation Method. *Exp. Mech.* **55**, 77–94 (2015).
4. A. Buades, B. Coll, J. Morel, The Staircasing Effect in Neighborhood Filters and its Solution. *IEEE Trans. Image Process.* **15**, 1499–1505 (2006).
5. A. Buades, B. Coll, J. Morel, Nonlocal Image and Movie Denoising. *Int. J. Comput. Vis.* **76**, 123–139 (2008).
6. Y. Tal, V. Rubino, A. J. Rosakis, N. Lapusta, Enhanced digital image correlation analysis of ruptures with enforced traction continuity conditions across interfaces. *Appl. Sci.* **9**, 1–17 (2019).